Archives of Biochemistry and Biophysics 772 (2025) 110569

Contents lists available at ScienceDirect

Archives of Biochemistry and Biophysics

journal homepage: www.elsevier.com/locate/yabbi

Brief communication

Sacsin deletion decreases cell viscoelasticity and motility in a glial cell model of autosomal recessive spastic ataxia of Charlevoix Saguenay

Fernanda Murtinheira [a,b,1], João Belo [a,c,1], Ana Sofia Boasinha [a,b], Tiago T. Robalo [a,c], Vukosava M. Torres [a,b], Francisco R. Pinto [a,b], Constança Pimenta [a,b], Patricia Nascimento [a,b], Mario S. Rodrigues [a,c,*], Federico Herrera [a,b,**]

[a] BioISI – Instituto de Biosistemas e Ciências Integrativas, Faculdade de Ciências da Universidade de Lisboa, 1749-016, Lisbon, Portugal
[b] Departamento de Química e Bioquímica, Faculdade de Ciências, Universidade de Lisboa, 1749-016, Lisboa, Portugal
[c] Departamento de Física, Faculdade de Ciências, Universidade de Lisboa, 1749-016, Lisboa, Portugal

ARTICLE INFO

Handling Editor: J.P. Jin

Keywords:
Sacsin
Intermediate filaments
Nestin
Plectin
Golgi apparatus
Atomic force microscopy
Viscoelasticity
ARSACS

ABSTRACT

Autosomal recessive spastic ataxia of Charlevoix-Saguenay (ARSACS) is a movement disorder caused by loss-of-function mutations in the sacsin gene. The most common hallmark of this disease is the disruption of intermediate filament networks in cells as diverse as neurons, kidney cells, fibroblasts, astroglia and microglia. Intermediate filaments are the main filaments responsible for the mechanical and viscoelastic properties of cells and tissues, but these have never been investigated in the context of ARSACS. Here, we analyzed the consequences of sacsin loss on the mechanical functions of astroglial-like C6 cells. The phenotype of $C6^{Sacs-/-}$ cells was analyzed by immunocytochemistry, electron microscopy, mass spectrometry, atomic force microscopy and motility/proliferation assays. $C6^{Sacs-/-}$ cells presented an abnormal cytoskeletal and organelle distribution, global proteome alterations linked to cell motility and mechanics, a significant decrease in cell elasticity in the cytoplasm, and a striking reduction in cell motility. These mechanical alterations in glial-like cells could be especially relevant for neuroinflammation and glial scar formation upon CNS injury. Our results support a possible role for alterations in glial functions in ARSACS and provide new tools for understanding the glial-specific mechanisms involved in this movement disorder.

1. Introduction

Loss-of-function mutations in the Sacsin chaperone cause autosomal recessive spastic ataxia of Charlevoix-Saguenay (ARSACS), a rare movement disorder [1,2]. Sacsin is a very large, multidomain protein with sequence homology to molecular chaperones, suggesting a role in protein quality control and cytoskeletal regulation [3–5]. The presence of Ubiquitin-like and J domains in its structure originally suggested that sacsin could be integrated in the ubiquitin-proteasome system [6]. Later computational and structural analyses confirmed this suspicion, revealing nucleotide-binding ATPase activity similar to the chaperone HSP90 [7–11]. Additionally, sacsin loss could also affect proteostasis pathways in an indirect manner, as it induces the relocalization of chaperones (e.g., HSP70), ubiquitin, and autophagy-lysosome pathway proteins (Lamp2 and p62) and an increased autophagic flux [3]. We recently observed that sacsin loss produces an overexpression of the S100B protein in C6 rat glioblastoma cells, which also displays chaperone activity and partially compensates for sacsin function in these cells [12].

Although sacsin is generally described as a neuronal protein expressed at high levels in Purkinje cells, elevated expression levels have also been reported in astroglial and microglial cells [12–17]; and The Protein Atlas, Harmonizome and BrainRNASeq public databases], indicating a broader role for sacsin in central nervous system (CNS) cell types. ARSACS brains show indicators of neuroinflammation and astroglial reactivity [17], suggesting a possible role for glial cells in

* Corresponding author. Atomic Force Microscopy and Related Techniques Laboratory. Faculdade de Ciências (Edifício C8), Universidade de Lisboa, Rua Ernesto de Vasconcelos, 1600-548, Lisboa, Portugal.
** Corresponding author. Cell Structure and Dynamics Laboratory. Faculdade de Ciências (Edifício C8), Universidade de Lisboa, Rua Ernesto de Vasconcelos, 1600-548, Lisboa, Portugal.
E-mail addresses: mmrodrigues@fc.ul.pt (M.S. Rodrigues), fherrera@fc.ul.pt (F. Herrera).
[1] These authors contributed equally to this work.

https://doi.org/10.1016/j.abb.2025.110569
Received 11 March 2025; Received in revised form 3 July 2025; Accepted 24 July 2025
Available online 25 July 2025

ARSACS.

Astroglial cells become hypertrophic in response to CNS insults, and in severe cases, they proliferate, migrate and close the wound, forming a glial scar that prevents further damage [18]. These phenomena require resistant, flexible and dynamic structural and mechanical glial cell components. Intermediate filaments (IFs) play a significant role in maintaining the mechanical and viscoelastic properties of cells [19], which are important for a wide range of cellular functions, such as cell migration, division, and differentiation [20] and membrane organelle homeostasis [21–23]. Disruption of the IF cytoskeleton and membrane organelle distribution are largely the most common hallmarks in all cellular and animal models of ARSACS [3–5,12,14,15]. Loss of sacsin in patients' fibroblasts, HEK293 human kidney cells, HMC3 human microglial cells and C6 rat glioblastoma cells induces juxtanuclear accumulation of the IF vimentin [3,12,14,15] and produces a relocalization of the proteostasis machinery (e.g. ubiquitin, HSP70, Lamp2, p62/SQSTM1) to these IF accumulates [3]. Alterations in IF networks are associated with at least 80 different human pathologies, some of which are similar to ARSACS and involve astroglial dysfunction, such as Alexander's disease and giant axonal neuropathy [24,25].

Here, we extend our previous observations on the C6 astroglial-like model of ARSACS [12,14], reporting a series of biochemical and biophysical alterations in mechanical structures upon sacsin loss-of-function that could be relevant to glial dysfunction in ARSACS.

2. Methods

1 Cell Cultures

C6 (rat, glioblastoma, astroglial-like) cells were acquired from ATCC (Ref. CCL-107). Cells were maintained in DMEM medium supplemented with 10 % v/v Fetal Bovine Serum (FBS), 1 % L-glutamine and 1 % Penicillin and Streptomycin mix and maintained at 37 °C in a 5 % CO_2 atmosphere. Sacsin knockout was achieved as previously described, using a CRISPR/Cas9 tool commercially available (Santa Cruz Biotechnologies) and a FACSAria III cell sorter (BD Biosciences) [14,15]. Cells were plated on different sterile plastic dishes or on sterile glass coverslips and allowed to adhere for 16–24 h before experiments and/or sample preparation. When indicated, cells were transfected 24 h after seeding with mammalian expression plasmids to visualize Golgi (EYFP-Golgi7, Addgene, # 56590), using JetPRIME transfection reagent (Polyplus transfection, Illkirch, France) at 1:3 transfection ratios.

2. Fluorescence Microscopy

Cells grown on coverslips on 24-well plates were washed with Dulbecco's Phosphate Buffered Saline (DPBS; San Marcos, TX, USA) and fixed with methanol for 15 min at −20 °C. Cells were then washed with DPBS (3 × 5 min) and permeabilized with 0.1 % Triton X-100 in DPBS for 10 min. After 3 washes with DPBS, cells were blocked with 1 % BSA in DPBS-T for 1 h at room temperature. Afterwards, incubation with primary antibodies (1:1000) against Nestin (sc-33677, Santa Cruz Biotechnologies) or Plectin (sc-33649, Santa Cruz Biotechnologies) was carried out overnight at 4 °C in a dark wet chamber. Cells were washed with DPBS for 5 min and incubated with the corresponding Alexa Fluor-conjugated secondary antibodies for 2 h at room temperature. Nuclei were counterstained with Hoechst 33342 (Molecular Probes, Willow Creek Rd Eugene, OR, USA); mitochondria with Mitoview™ Fix 640 (Biotium; Fremont, CA, USA); actin with SiR-actin (Spirochrome); and tubulin with Tubulin Tracker (Invitrogen). The coverslips were mounted on microscopy slides and imaged using a Leica DMI4000B widefield Microscope, equipped with a x63 oil objective HCX PL APO and a Leica DFC365 FX 1.4 MP CCD camera (6.45 × 6.45 μm/pixel). Images were analyzed with the ImageJ/Fiji software (Rasband, W.S., ImageJ, U. S. National Institutes of Health, Bethesda, Maryland, USA, https://imagej.net/ij/, 1997–2018). Golgi scattering was measured as the percentage of cells showing ring-like distribution, number of distinguishable Golgi fragments and area of these fragments. Plectin redistribution was measured by the percentage of cells showing absence of plectin in the perinuclear area, and by the loss of fluorescence in this area.

3. Electron Microscopy

The preparation of samples and imaging by transmission electron microscopy were performed at the Electron Microscopy Facility at the Gulbenkian Institute for Molecular Medicine. Briefly, cells were grown for 24 h on coverslips and fixed on 2 % w/v formaldehyde/2.5 % w/v glutaraldehyde in 0.1 M phosphate buffer pH 7.4 for 45 min on ice. Samples were then washed with 0.1 M phosphate buffer three times, and post-fixed with 1 % w/v OsO_4/1.5 % K ferro for 30 min on ice in the dark. Samples were washed and stained with 1 % Tannic acid for 20 min on ice, washed and incubated with 0.5 % uranium acetate for 1 h at room temperature in the dark. Samples were dehydrated in increasing concentrations of ethanol and then infiltrated and embedded in Epon resin. The resulting blocks were then cut into 70 nm thick sections using a Leica UC7 ultramicrotome equipped with a Diatome diamond knife. These sections were subsequently mounted onto copper slot grids coated with formvar and carbon. Pictures were taken in a FEI Tecnai G2 Spirit BioTWIN (120 keV) microscope equipped with an Olympus-SIS Veleta CCD Camera.

4. Total protein extraction

Cells seeded in 35 mm dishes were washed with DPBS (Cytiva; Marlborough, MA, USA) and lysed using a Native lysis buffer (150 mM NaCl, 50 mM Tris-HCl pH 7.4/7.5) supplemented with cocktails of protease inhibitors (Protease Inhibitor cocktail EDTA free, Abcam, Cambridge, UK) and phosphatase inhibitors (Halt Phosphatase Inhibitor Single-use cocktail, Thermo Fisher Scientifics, Waltham, MA, USA). Cells were scraped from the surfaces of the plates into microcentrifuge tubes and incubated for 10 min in ice. A UP200s sonicator (Hielscher Ultrasonics GmbH, Teltow, Germany) was used to disrupt cell membranes for 10 s to release intracellular proteins. Cells were then centrifuged at 10,000×*g* for 10 min at 4 °C and the soluble protein fraction was collected. Protein concentration was quantified by the Bradford method on a 96-well plate (Orange Scientific; Braine-l'Alleud, Belgium). A standard curve with known concentrations of bovine serum albumin (BSA, 0.125–2 μg/μL) was used to determine protein concentration. Samples were incubated with 200 μL of Bradford solution (Alfa Aesar, Ward Hill, MA, USA) for 5 min and then read at 595 nm in the absorbance microplate reader Sunrise (Tecan, Männedorf, Switzerland).

5. Mass spectrometry

Label-free proteomics [26,27] was conducted on C6 and C6$^{Sacs-/-}$ native protein extracts to identify possible alterations in our glial cell model of ARSACS. Briefly, total protein samples (20 μg) were diluted with 8 M urea in 100 mM ammonium bicarbonate (pH 7.8) and processed via Nanosep™ filters (10 kDa cutoff), with buffer exchange performed over five cycles (200 μL, 12,000 rpm, 5 min). Reduction was carried out with 100 mM DTT (56 °C, 50 min), followed by alkylation with 500 mM IAA (30 min in the dark). The buffer was then replaced with 100 mM ammonium bicarbonate (four cycles). Proteolysis was performed via trypsin/LysC (1:50 enzyme-to-substrate ratio) at 37 °C for 16 h. Peptides were sequentially eluted with 100 mM ammonium bicarbonate and 0.5 % formic acid, concentrated via a SpeedVac and cleaned with in-house C18 stage tips. The final peptides were stored in 5 % acetonitrile/0.1 % formic acid for LC/MS analysis. Peptides were analyzed via a nano Elute™ UHPLC coupled with an Impact II™ QqTOF-MS. Separation was achieved on a Bruker fifteen™ column with a 120 min gradient (300 nL/min, 40 °C). Mass-specific acquisition was performed in data-dependent mode with a 3-s cycle, and the spectra

were recalibrated via sodium formate. The raw MS data were processed in MaxQuant (v2.2.0.0) against the UniProt *Rattus norvegicus* database (<1 % FDR) [23]. Fixed modifications included carbamidomethylation, whereas oxidation and acetylation were variable. Label-free quantification (LFQ) normalization was performed with a minimum ratio of 2. LFQ values were used to quantify proteins with at least two LFQ values in one replicate group and more than one unique peptide. The log2-transformed LFQ values were normalized to the median number of proteins detected in all the samples. Missing value imputation was applied with the knn algorithm (1 missing replicate) or with the minimum LFQ of each sample (>1 missing replicate). Differential expression was tested with the limma R package [28]. Adjusted p values < 0.05 were considered significant. The R code is available at https://github.com/GamaPintoLab/sacsin/. Functional enrichment analysis was performed with the Database for Annotation, Visualization and Integrated Discovery (DAVID, https://david.ncifcrf.gov/).

6. Atomic Force Microscopy

The elasticity of 211 C6 cells and 168 $C6^{Sacs-/-}$ cells from 6 independent experiments was analyzed via atomic force microscopy with a PicoLE Molecular Imaging system from Agilent Technologies (Keysight Technologies, Inc., Santa Rosa, CA, USA). CP-qp-SCONT-SiO-A nanoelectrode cantilevers with a nominal stiffness of 0.01 N/m and a nominal tip radius of 1 μm were used in all the experiments. To reduce bias due to different cantilever stiffnesses, the same cantilevers were used to measure both C6 and $C6^{Sacs-/-}$ cells in each experiment. To measure the mechanical properties of full cell bodies, we used grids of 32 × 32 approach/retract force–displacement curves in the range of approximately 30 μm. To determine the Young's modulus (E_0) of the cells, we used the Hertz contact model to fit the contact portion of the approach force curve, as explained elsewhere [29].

7. Migration assays

For wound healing assays, C6 and $C6^{Sacs-/-}$ cells were seeded into 35 mm glass bottom dishes in a standard growth medium. Cells were allowed to adhere for 16–24 h, and then the confluent monolayer was gently scratched across the centre of the dish with a sterile pipette tip (Ø = 0.1 mm) and washed with PBS. The scratch-injured cells were incubated at 37 °C and 5 % CO_2. The wound healing was evaluated using phase-contrast images acquired at 0, 5 and 24 h post-scratch with a Leica DMI6000 B widefield Microscope equipped with a x20 objective HC PL FLUOTAR and a Monochrome CMOS camera 4.0 MP (2048 x 2048 pixels). We determined the scratch area with the Wound_healing_size_tool plugin of ImageJTM software [30]. We calculated the percentage of wound closure according to the equation:

$$Wound\ Closure\% = \left(\frac{A_{t=0} - A_{t=\Delta t}}{A_{t=0}}\right) x100\%$$

Where $A_{t=0}$ is the initial wound area, $A_{t\ =\ \Delta t}$ is the wound area after n hours of the initial scratch, both in μm^2.

Transwell assays were carried out as previously described [31], with small modifications: Cells had serum-free DMEM in the inner chamber and complete medium in the outer chamber, using FBS as chemoattractant to promote cell migration; and cells were fixed 24 h later with paraformaldehyde 4 % w/v instead of ethanol (70 % v/v). For imaging, cells were stained with Hoechst, as described above, and visualized at 20× magnification.

8. Cell cycle analysis

For cell cycle analysis, C6 and $C6^{Sacs-/-}$ cells were seeded in 6-well plates (5×10^5 cells/well) in a standard growth medium for 48 h. Adherent cells were collected by trypsinization and centrifugation, and fixed by adding ice-cold 70 % ethanol dropwise and incubating overnight at 4 °C. Cells were centrifuged at 500×*g* for 5 min, washed twice with PBS, and resuspended in a propidium iodide solution (50 μg/ml in PBS) containing RNase A (100 μg/ml). After 20 min of incubation at 37 °C, cells were analyzed using a FACSCalibur flow cytometer (BD Biosciences, Franklin Lakes, NJ, USA). Ten thousand events were recorded for cell cycle analysis with the Floreada online software (https://floreada.io/).

3. Results and discussion

Sacsin deletion in C6 cells induces disorganization and juxtanuclear accumulation of the three main glial IFs [14], and here we use nestin as a surrogate (Fig. 1A). The Golgi apparatus also becomes dispersed upon sacsin deletion, becoming distributed around IF aggregates (Fig. 1A and B). Near 60 % of cells show nestin accumulation and Golgi scattering, and the Golgi apparatus undergoes an apparent fragmentation in smaller vesicles (Fig. 1B and C). These results reproduce perfectly previous reports analyzing the consequences of sacsin loss in ARSACS patient fibroblasts and HEK293 cells [3].

Plectin, a crucial linker protein between IFs and various cellular components, has been identified as a sacsin interactor, and its distribution is altered by sacsin loss in Purkinje cells, fibroblasts and SHSY5Y cells [17]. In our $C6^{Sacs-/-}$ model, plectin also showed a change in its cellular distribution, being absent from the juxtanuclear region where the IFs accumulate in 40 % of cells, similar to mitochondria (Fig. 1D and E). This finding is consistent with reports showing that plectin colocalizes with mitochondria in striated muscle [22] or directly binds to both vimentin and mitochondria [21]. We do not observe major alterations in actin or tubulin distribution or morphology (Suppl. Fig. 1), certainly nothing as striking as the disorganization of IFs, plectin and membrane organelles. However, we cannot rule out more subtle changes in either structure or dynamics of microfilaments and microtubules. Our results suggest that juxtanuclear IF accumulation pushes plectin, mitochondria and the Golgi apparatus out of dense IF bundles.

Such striking structural changes could either produce or be indicative of global molecular alterations in $C6^{Sacs-/-}$ cells, as has been observed in other cell and animal models of ARSACS [33–36]. In order to characterize possible global alterations in our glial cell model, we carried out mass spectrometry analysis of total proteins from C6 and $C6^{Sacs-/-}$ cells in three independent cultures. To avoid bias due to variability between experiments, we focused our analysis only in those proteins that were common to the three independent replicates (Suppl. Fig. 2A). After removal of redundant hits, we identified 1552 proteins by mass spectrometry: 1490 common to both C6 and $C6^{Sacs-/-}$ cells, 103 unique to C6 reference cells and 30 exclusive to $C6^{Sacs-/-}$ cells (Suppl. Fig. 2A). Among these, the expression of 140 proteins significantly differed between C6 and $C6^{Sacs-/-}$ cells: 104 were downregulated, and 36 were upregulated (Fig. 1F, Suppl. Fig. 2B and C). Differentially expressed proteins were further analyzed by functional enrichment of gene ontology terms (a full list is provided in Suppl. Fig. 3).

The differentially expressed proteins were enriched in processes such as cell adhesion and migration, the cellular response to mechanical stimuli or the negative regulation of cell proliferation (Fig. 1G). In the cellular component, differentially expressed proteins play a role in structural integrity (e.g., cytoskeleton, filopodium, podosomes and stress fibers) and cellular connection and communication (e.g., cell–cell adherens junctions and focal adhesion proteins) (Fig. 1H). Filopodia, podosomes and stress fibers are structures closely related to actin microfilaments [32], and therefore the hypothesis that microfilament dynamics are somewhat altered deserves a more detailed analysis in the future. These results are consistent with disorganization of the IF networks and alterations in the mechanical properties of cells and resemble the proteome and transcriptome profiles found in other cell and animal models of ARSACS [33–36].

IFs are essential for maintaining the mechanical and viscoelastic

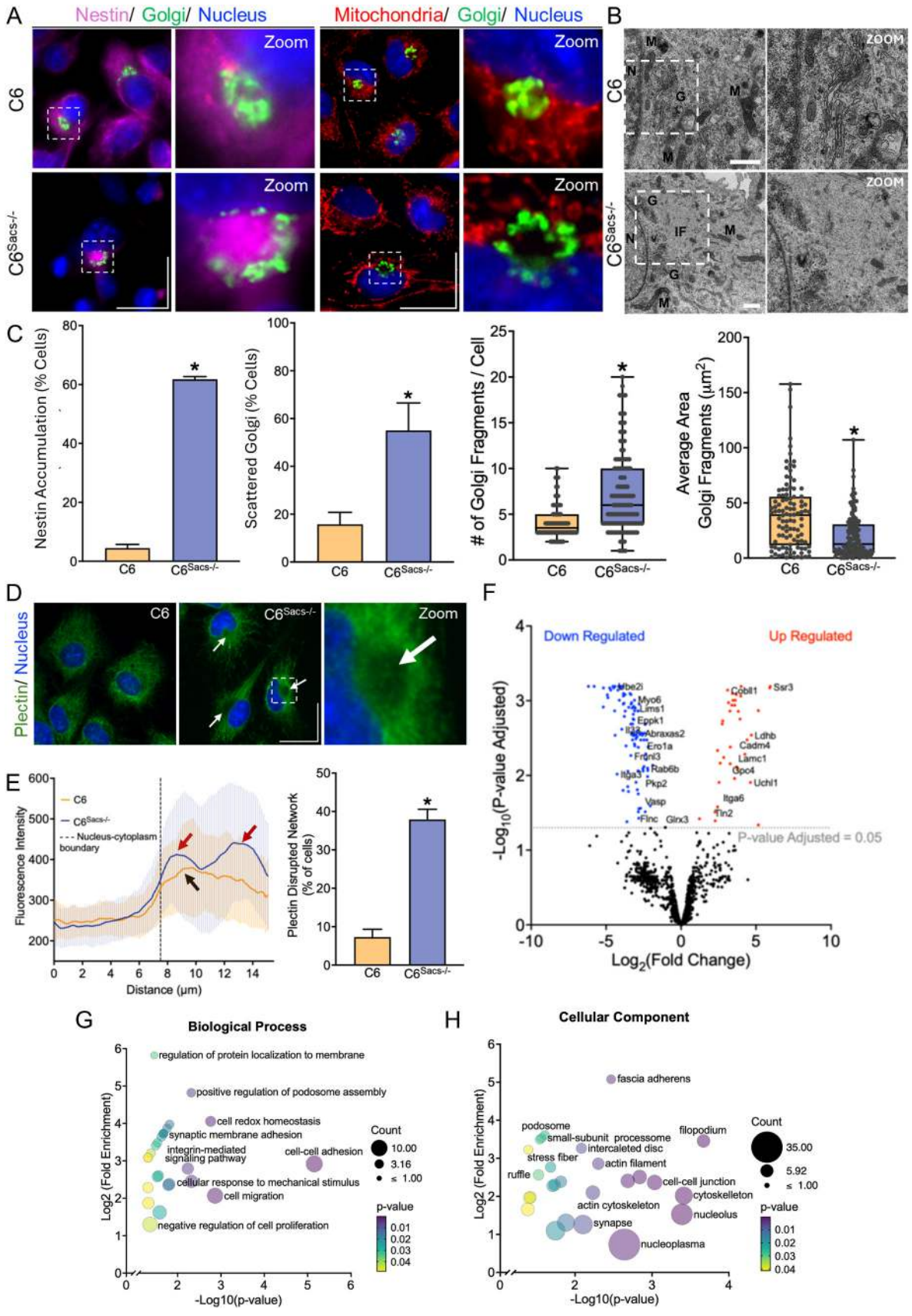

(caption on next page)

Fig. 1. Sacsin deletion causes severe cytoskeletal-related alterations in C6 astroglial-like cells. (A,B) Representative immunofluorescence (A) and electron microscopy (B) images showing the distribution of Golgi apparatus, mitochondria, and intermediate filaments in C6 and C6$^{Sacs-/-}$ cells. Cells were transfected with EYFP-Golgi7 (green) and immunostained with an antibody against nestin (magenta). Mitochondria (red) and nuclei (blue) were counterstained as described in Methods. Scale bars, 20 μm (immunofluorescence) and 1 μm (electron microscopy. Regions in white squares were magnified (Zoom) to exemplify normal and scattered Golgi distribution in both immunofluorescence and electron microscopy images. (C) Graphs show the mean ± SEM of at least 3 independent experiments, as indicated. Nestin: n = 4, a total of 588/995 C6/C6$^{Sacs-/-}$ cells. Golgi: n = 3, 344/322 C6/C6$^{Sacs-/-}$ cells. Morphometric analysis of EYFP-Golgi7–labeled Golgi fragments was performed using the "Analyze Particles" plugin in ImageJ. (D) Representative immunofluorescence images showing the distribution of plectin in C6 and C6$^{Sacs-/-}$ cells. (E) Line scan analysis of plectin fluorescence intensity along the nuclear-cytoplasmic axis (0–15 μm), performed using the "Plot Profile" plugin in Fiji (ImageJ). The black dashed line marks the nuclear–cytoplasmic boundary at 7.5 μm. Graph shows the mean fluorescence intensity ± SD of C6 (orange) and C6$^{Sacs-/-}$ (blue) cells (n = 61 cells per group). C6$^{Sacs-/-}$ cells exhibit elevated cytoplasmic plectin intensity with two distinct peaks (red arrows), whereas C6 cells display a single peak (black arrow), indicating altered plectin subcellular distribution following SACS deletion. A statistically significant difference in fluorescence intensity was detected in the peripheral cytoplasm (position >12 μm), as determined by two-way ANOVA followed by Holm–Šídák's multiple comparisons test. (n = 3, 464/697 C6/C6$^{Sacs-/-}$ cells). Cells with this altered plectin distribution were quantified and represented in the bar graph. *, significant vs. C6 reference strain ($p < 0.05$, Student's t-test). (F) Differentially expressed proteins. Black, unchanged proteins; red, upregulated; blue, downregulated; the horizontal dashed line indicates adjusted p-value = 0.05. (G, H) Functional Enrichment Analysis of Gene Ontology terms. Terms with adjusted p values < 0.05 were selected.

properties of cells [19,20], but these properties have never been tested in ARSACS models. This approach allowed us to produce a topology map, i.e., the height of the different sections of the cell body a given amount (Fig. 2A), as well as an elasticity map, i.e. a measure of the pressure needed to deform the different sections of the cell body (Fig. 2B), for each cell. The highest point of the cells corresponded to the location of the nucleus, which later served as a reference for comparison. In Fig. 2C, R is the radial distance from the highest point. We thus confirmed a significant decrease in the apparent Young's modulus of C6$^{Sacs-/-}$ cells as we moved farther from the nucleus. When the radius R was lower than 5 μm around the highest point (Fig. 2C, top graph), which was still on top of the nuclei, elasticity was similar in both cell strains. When the radius is less than 10 μm, including the perinuclear region of the cytoplasm, elasticity is already significantly lower in cells lacking sacsin. The difference in elasticity reaches its maximum beyond this region in the cytoplasm (Fig. 2C, bottom graph). These results further support the structural alterations we described in the cytoplasmic cytoskeleton, leading to lower elasticity and greater stiffness of the cytoplasmic regions. In contrast, the elasticity of the nuclear region, which is supported mainly by nuclear lamin IFs, seems unaffected by sacsin loss. This is consistent with no overt changes in lamin B distribution (Suppl. Fig. 4), although we cannot rule out more subtile alterations in nuclear IF dynamics.

The widespread mechanical and cytoskeletal alterations described in C6 cells upon sacsin loss could strongly impact cell proliferation and motility, and these astroglial functions are especially relevant in severe neuroinflammation [18]. To evaluate this possibility, we carried out migration assays (Wound healing and Transwell) and cell cycle analysis of C6 and C6$^{Sacs-/-}$ cells. Consistently, C6$^{Sacs-/-}$ cells presented a significantly delayed wound closure response already 5 h after scratch (Fig. 2D and E), when the contribution of proliferation should be minimal in comparison to migration events. This delayed response is maintained after 24 h (Fig. 2D and E). Transwell assays, where the capability of cells to go through 5 μm pores is measured, confirmed the alteration in cell motility in C6$^{Sacs-/-}$ cells (Fig. 2D–F).

Finally, a decrease in the proportion of cells in the G0/G1 phase and a greater proportion of cells in the G2/M phase was also observed 48 h after seeding (Fig. 2G). These results strongly suggest that sacsin loss disrupts both C6 proliferation and motility.

To the best of our knowledge, this is the first time that changes in cell topography, viscoelasticity and motility are reported in the context of ARSACS. Sacsin loss-of-function systematically and reproducibly disrupts IF networks [3–6,12,14,15], and IF networks are the main responsible for the viscoelastic properties of cells [19,20]. IFs form a flexible cage that provides mechanical resistance to both cells and tissues, but also contributes to cell motility [19,20]. Silencing of vimentin, nestin and/or GFAP inhibits proliferation and migration of primary astroglia and cancer cells [37–39]. Cell migration is a major phenomenon during CNS development, as neural precursor cells often produce new cells far from their final destination [40]. ARSACS is an early onset disease, with symptoms appearing early after birth [1,2], and ARSACS brains are therefore expectable to have -yet undetected-alterations before birth. If sacsin loss disrupts neural precursor cell motility, this could have dire and early consequences in CNS function. IFs are also involved in neuroinflammation, another process where cell motility plays a key role [18], and neuroinflammation has been observed in later stages of ARSACS mice [17]. Our results could lay the groundwork for future studies in this direction in embryonic stages of ARSACS mice.

In summary, our results support the idea that widespread alterations in the cytoskeletal networks in our glial cell model of ARSACS have biologically relevant, deleterious consequences on the mechanical properties of cells, including proliferation and motility. These properties of glial cells are key during CNS development and neuroinflammation and glial scar formation, and point to a possible role for glial cell dysfunction in ARSACS. Further analysis of the glial-specific functions of sacsin should be carried out to determine the extent of its contribution to ARSACS symptoms and histopathological features.

CRediT authorship contribution statement

Fernanda Murtinheira: Writing – review & editing, Methodology, Investigation, Formal analysis. **João Belo:** Methodology, Investigation, Formal analysis. **Ana Sofia Boasinha:** Visualization, Methodology, Investigation, Formal analysis. **Tiago T. Robalo:** Visualization, Validation, Methodology, Investigation, Formal analysis, Data curation. **Vukosava M. Torres:** Visualization, Validation, Supervision, Resources, Methodology, Investigation, Formal analysis. **Francisco R. Pinto:** Visualization, Validation, Supervision, Software, Methodology, Investigation, Formal analysis. **Constança Pimenta:** Writing – review & editing, Methodology, Investigation. **Patricia Nascimento:** Investigation. **Mario S. Rodrigues:** Validation, Supervision, Software, Methodology, Funding acquisition, Formal analysis. **Federico Herrera:** Writing – review & editing, Writing – original draft, Supervision, Project administration, Funding acquisition, Conceptualization.

Funding

We acknowledge support from the BioISI/FCUL Microscopy Facility, a node of the Portuguese Platform of BioImaging (PPBI–POCI-01-0145-FEDER-022122); the BioISI MS facility, which is supported by center grants https://doi.org/10.54499/UIDP/04046/2020 and https://doi.org/10.54499/UIDB/04046/2020; and the Portuguese MS Network, which is integrated into the National Roadmap of Research Infrastructures of Strategic Relevance (ROTEIRO/0028/2013; LISBOA-01-0145-FEDER-022125). We acknowledge Michael J. Hall and Ana Laura Vinagre from the Electron Microscopy Facility at the Gulbenkian Institute for Molecular Medicine for their help in sample processing and imaging. We would also like to thank the flow cytometry facilities at the Gulbenkian Institute of Molecular Medicine (Lisbon and Oeiras, Portugal) for their technical support. FH, VMT, FRP and MSR were

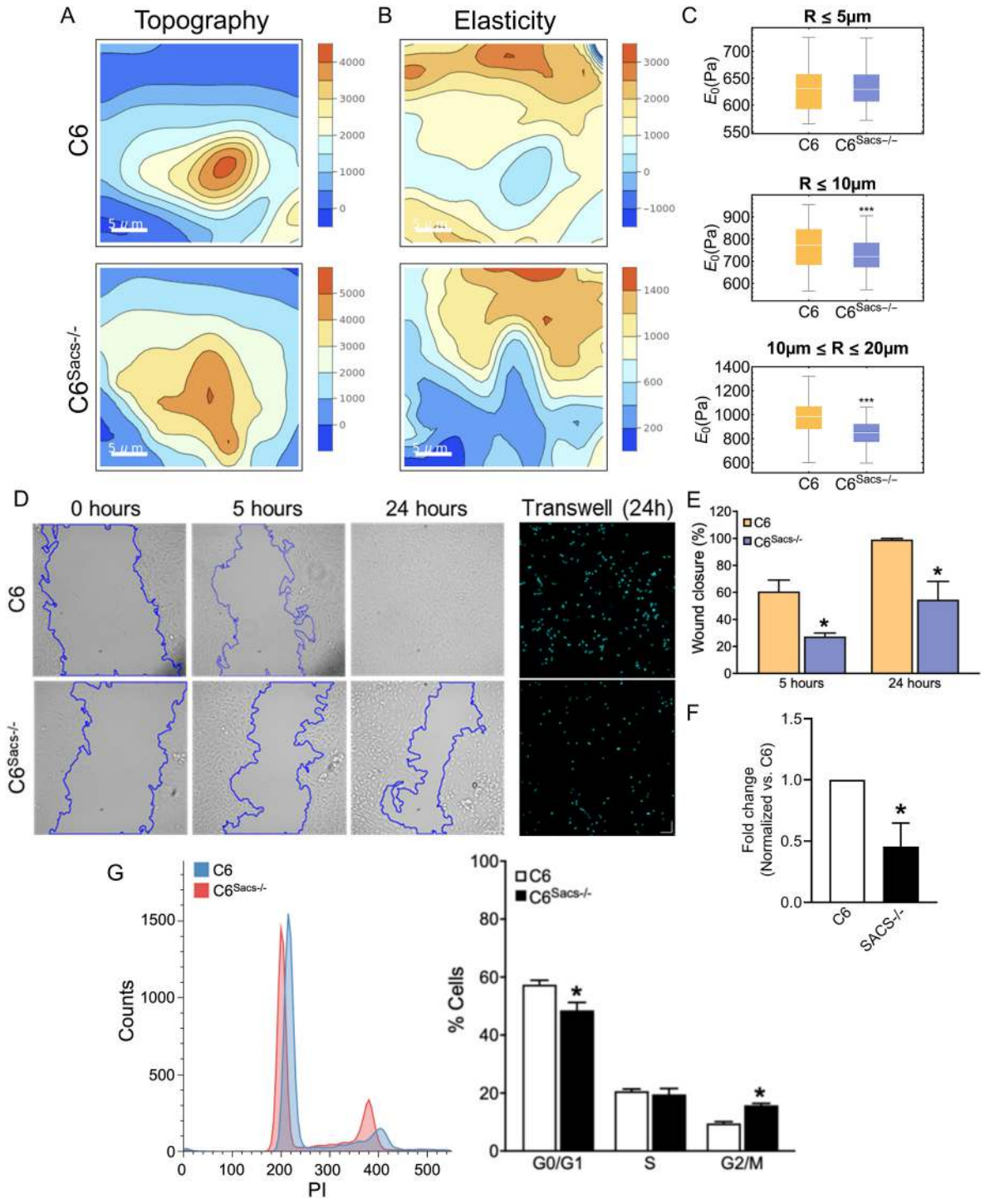

Fig. 2. Mechanical alterations caused by sacsin loss and IF disorganization in C6 cells. (A) Topology of representative C6 and C6$^{Sacs-/-}$ cells. The color code of the contour plot indicates height (Z dimension) in nm. The X and Y axis indicate distance in these two horizontal dimensions in μm. (B) Contour Plot of the elasticity modulus (in Pascals, Pa) of representative C6 and C6$^{Sacs-/-}$ cells in (A). The X and Y axis indicate distance in these two horizontal dimensions in μm. Scale bar, 5 μm. (C) Elastic modulus (E0, in Pascals) obtained within a radius of 5 μm (top graph), 10 μm (middle graph) and between 10 and 20 μm (bottom graph) from the cell top, respectively. R = distance from the cell top. (D) Representative microscopy images were acquired at 0, 5 and 24 h after scratch (Wound healing assays, Scale bar, 75 μm) or 24 h after seeding (Transwell assays, Scale bar, 100 μm). (E) Quantification of the percentage of wound closure 5 and 24 h after scratch (n = 3, mean ± SEM), by means of the Wound healing size tool plugin of ImageJTM software. (F) Quantification of the proportion of cells crossing the 5 μm pore membranes versus reference C6 cells. (G) Representative cell cycle profiles of C6 and C6$^{Sacs-/-}$ cells based on the intensity of DNA staining by propidium iodide; and quantitative analysis of the distribution of the cells in each phase of the cell cycle. Data are represented as the mean ± SEM (n = 4). *, significant vs. C6 reference strain ($p < 0.05$, Student's *t*-test). Flow cytometry data were analyzed by means of Floreada online software (https://floreada.io/).

supported by center grants https://doi.org/10.54499/UIDP/04046/2020, https://doi.org/10.54499/UIDB/04046/2020, UID/00100 (DOI: 10.54499/UIDB/04046/2020) and UID/04046/2025 (BioISI Research Unit) and individual grants (Refs. PTDC/BTM-TEC/28554/2017, https://doi.org/10.54499/PTDC/FIS-MAC/2741/2021 and 2023.14971.PEX to VMT, MSR and FH, respectively) through Fundação para a Ciência e Tecnologia. FH was supported by a grant from the ARSACS Foundation (Canada), which included a fellowship to ASB, and two small grants from Ataxia UK (United Kingdom). FM and ASB were also supported by FCT PhD fellowships (Refs. SFRH/BD/133220/2017 and 2024.02710.BD). Funded by the European Union (TWIN2PIPSA, GA 101079147). The views and opinions expressed are, however, those of the author(s) only and do not necessarily reflect those of the European Union or European Research Executive Agency (REA). Neither the European Union nor the granting authority can be held responsible for them. The authors have no other financial disclosures to make for the past year.

Conflict of interest

The authors declare that they have no conflicts of interest. The funders had no role in the design of the study; in the collection, analyses, or interpretation of data; in the writing of the manuscript; or in the decision to publish the results.

Appendix A. Supplementary data

Supplementary data to this article can be found online at https://doi.org/10.1016/j.abb.2025.110569.

Data availability

Data will be made available on request.

References

[1] R. Larivière, R. Gaudet, B.J. Gentil, et al., Sacs knockout mice present pathophysiological defects underlying autosomal recessive spastic ataxia of charlevoix-saguenay, Hum. Mol. Genet. 24 (3) (2015) 727–739, https://doi.org/10.1093/hmg/ddu491.

[2] S. Vermeer, B. P. van de Warrenburg, E.-J. Kamsteeg, B. Brais, M. Synofzik, ARSACS, J. Neurol. Sci. 455 (2020) 121002, https://doi.org/10.1016/j.jns.2023.121002.

[3] E.J. Duncan, R. Larivière, T.Y. Bradshaw, et al., Altered organization of the intermediate filament cytoskeleton and relocalization of proteostasis modulators in cells lacking the ataxia protein sacsin, Hum. Mol. Genet. 26 (16) (2017) 3130–3143, https://doi.org/10.1093/hmg/ddx197.

[4] B.J. Gentil, G.-T. Lai, M. Menade, et al., Sacsin, mutated in the ataxia ARSACS, regulates intermediate filament assembly and dynamics, FASEB J. 33 (2) (2018) 2982–2994, https://doi.org/10.1096/fj.201801556R.

[5] A. Dabbaghizadeh, A. Paré, Z. Cheng-Boivin, et al., The J domain of sacsin disrupts intermediate filament assembly, Int. J. Mol. Sci. 23 (24) (2022) 15742, https://doi.org/10.3390/IJMS232415742/S1.

[6] D.A. Parfitt, G.J. Michael, E.G. Vermeulen, N.V. Prodromou, T.R. Webb, J.M. Gallo, M.E. Cheetham, W.S. Nicoll, G.L. Blatch, J.P. Chapple, The ataxia protein sacsin is a functional co-chaperone that protects against polyglutamine-expanded ataxin-1, Hum. Mol. Genet. 18 (9) (2009 May 1) 1556–1565, https://doi.org/10.1093/hmg/ddp067.

[7] J.F. Anderson, E. Siller, J.M. Barral, The neurodegenerative-disease-related protein sacsin is a molecular chaperone, J. Mol. Biol. 411 (4) (2011 Aug 26) 870–880, https://doi.org/10.1016/j.jmb.2011.06.016.

[8] J.F. Anderson, E. Siller, J.M. Barral, The sacsin repeating region (SRR): a novel Hsp90-related supra-domain associated with neurodegeneration, J. Mol. Biol. 400 (4) (2010 Jul 23) 665–674, https://doi.org/10.1016/j.jmb.2010.05.023.

[9] A. Romano, A. Tessa, A. Barca, F. Fattori, M.F. de Leva, A. Terracciano, C. Storelli, F.M. Santorelli, T. Verri, Comparative analysis and functional mapping of SACS mutations reveal novel insights into sacsin repeated architecture, Hum. Mutat. 34 (3) (2013 Mar) 525–537, https://doi.org/10.1002/humu.22269.

[10] M. Ménade, G. Kozlov, J.F. Trempe, H. Pande, S. Shenker, S. Wickremasinghe, X. Li, H. Hojjat, M.J. Dicaire, B. Brais, P.S. McPherson, M.J.H. Wong, J.C. Young, K. Gehring, Structures of ubiquitin-like (Ubl) and Hsp90-like domains of sacsin provide insight into pathological mutations, J. Biol. Chem. 293 (33) (2018 Aug 17) 12832–12842, https://doi.org/10.1074/jbc.RA118.003939.

[11] L. Perna, M. Castelli, E. Frasnetti, L.E.L. Romano, G. Colombo, C. Prodromou, J. P. Chapple, AlphaFold predicted structure of the Hsp90-like domains of the neurodegeneration linked protein sacsin reveals key residues for ATPase activity, Front. Mol. Biosci. 9 (2023 Jan 13) 1074714, https://doi.org/10.3389/fmolb.2022.1074714.

[12] A.S. Boasinha, F. Murtinheira, S. Solá, C.M. Gomes, F. Herrera, S100B mitigates cytoskeletal and mitochondrial alterations in a glial cell model of autosomal recessive spastic ataxia of Charlevoix-Saguenay, Mol. Neurobiol. 19 (2025 May), https://doi.org/10.1007/s12035-025-05057-3.

[13] L.E. Clarke, S.A. Liddelow, C. Chakraborty, A.E. Münch, M. Heiman, B.A. Barres, Normal aging induces A1-like astrocyte reactivity, Proc. Natl. Acad. Sci. U. S. A 115 (8) (2018) E1896–E1905, https://doi.org/10.1073/PNAS.1800165115/-/DCSUPPLEMENTAL.

[14] F. Murtinheira, M. Migueis, R. Letra-Vilela, et al., Sacsin deletion induces aggregation of glial intermediate filaments, Cells 11 (2) (2022), https://doi.org/10.3390/cells11020299.

[15] F. Murtinheira, E. Farsetti, L. Macedo, A.S. Boasinha, M.S. Rodrigues, A. Fernandes, F. Herrera, A human microglial cell model of autosomal recessive spastic ataxia of Charlevoix-Saguenay, Biochim. Biophys. Acta Mol. Basis Dis. 1870 (8) (2024 Dec) 167452, https://doi.org/10.1016/j.bbadis.2024.167452.

[16] Y. Zhang, S.A. Sloan, L.E. Clarke, et al., Purification and characterization of progenitor and mature human astrocytes reveals transcriptional and functional differences with mouse, Neuron 89 (1) (2016) 37, https://doi.org/10.1016/J.NEURON.2015.11.013.

[17] A. Del Bondio, F. Longo, D. De Ritis, et al., Restoring calcium homeostasis in Purkinje cells arrests neurodegeneration and neuroinflammation in the ARSACS mouse model, JCI Insight 8 (12) (2023), https://doi.org/10.1172/JCI.INSIGHT.163576.

[18] A. Verkhratsky, A. Butt, B. Li, et al., Astrocytes in human central nervous system diseases: a frontier for new therapies, Signal Transduct. Targeted Ther. 8 (1) (2023 Oct 13) 396, https://doi.org/10.1038/s41392-023-01628-9.

[19] S. Sivaramakrishnan, J.V. DeGiulio, L. Lorand, R.D. Goldman, K.M. Ridge, Micromechanical properties of keratin intermediate filament networks, Proc. Natl. Acad. Sci. U. S. A 105 (3) (2008) 889–894, https://doi.org/10.1073/PNAS.0710728105/SUPPL_FILE/10728SUPPMETHODS.PDF.

[20] K. Pogoda, P.A. Janmey, Transmit and protect: the mechanical functions of intermediate filaments, Curr. Opin. Cell Biol. 85 (2023), https://doi.org/10.1016/J.CEB.2023.102281.

[21] L. Winter, C. Abrahamsberg, G. Wiche, Plectin isoform 1b mediates mitochondrion–intermediate filament network linkage and controls organelle shape, JCB (J. Cell Biol.) 181 (6) (2008) 903–911, https://doi.org/10.1083/JCB.200710151.

[22] S. Reipert, F. Steinböck, I. Fischer, R.E. Bittner, A. Zeöld, G. Wiche, Association of mitochondria with plectin and desmin intermediate filaments in striated muscle, Exp. Cell Res. 252 (2) (1999) 479–491, https://doi.org/10.1006/EXCR.1999.4626.

[23] T.Y. Bradshaw, L.E.L. Romano, E.J. Duncan, et al., A reduction in Drp1-mediated fission compromises mitochondrial health in autosomal recessive spastic ataxia of Charlevoix Saguenay, Hum. Mol. Genet. (2016), https://doi.org/10.1093/hmg/ddw173.

[24] M.B. Omary, "IF-pathies": a broad spectrum of intermediate filament–associated diseases, J. Clin. Investig. 119 (7) (2009) 1756, https://doi.org/10.1172/JCI39894.

[25] B. Renganathan, J.P. Zewe, Y. Cheng, et al., Gigaxonin is required for intermediate filament transport, FASEB J. 37 (5) (2023 May) e22886, https://doi.org/10.1096/fj.202202119R.

[26] J.R. Wiśniewski, A. Zougman, N. Nagaraj, M. Mann, Universal sample preparation method for proteome analysis, Nat. Methods 6 (5) (2009) 359–362, https://doi.org/10.1038/NMETH.1322.

[27] S. Tyanova, T. Temu, J. Cox, The MaxQuant computational platform for mass spectrometry-based shotgun proteomics, Nat. Protoc. 11 (12) (2016) 2301–2319, https://doi.org/10.1038/NPROT.2016.136.

[28] M.E. Ritchie, B. Phipson, D. Wu, Y. Hu, C.W. Law, W. Shi, G.K. Smyth, Limma powers differential expression analyses for RNA-sequencing and microarray studies, Nucleic Acids Res. 43 (7) (2015) e47, https://doi.org/10.1093/NAR/GKV007.

[29] A.P. Carapeto, M.V. Vitorino, J.D. Santos, et al., Mechanical properties of human bronchial epithelial cells expressing Wt- and mutant CFTR, Int. J. Mol. Sci. 21 (8) (2020) 2916, https://doi.org/10.3390/IJMS21082916, 2020.

[30] A. Suarez-Arnedo, F. Torres Figueroa, C. Clavijo, P. Arbeláez, J.C. Cruz, C. Muñoz-Camargo, An ImageJ plugin for the high throughput image analysis of in vitro scratch wound healing assays, PLoS One 15 (7) (2020 Jul 28) e0232565, https://doi.org/10.1371/journal.pone.0232565.

[31] C.R. Justus, M.A. Marie, E.J. Sanderlin, L.V. Yang, Transwell in vitro cell migration and invasion assays, Methods Mol. Biol. 2644 (2023) 349–359, https://doi.org/10.1007/978-1-0716-3052-5_22.

[32] I.M. Antón, G.E. Jones, F. Wandosell, R. Geha, N. Ramesh, WASP-interacting protein (WIP): working in polymerisation and much more, Trends Cell Biol. 17 (11) (2007 Nov) 555–562, https://doi.org/10.1016/j.tcb.2007.08.005.

[33] L.E.L. Romano, W.Y. Aw, K.M. Hixson, et al., Multiomic profiling reveals the ataxia protein sacsin is required for integrin trafficking and synaptic organization, Cell Rep. 41 (5) (2022 Nov 1) 111580, https://doi.org/10.1016/j.celrep.2022.111580.

[34] F. Morani, S. Doccini, G. Chiorino, et al., Functional network profiles in ARSACS disclosed by aptamer-based proteomic technology, Front. Neurol. 11 (2021 Jan 27) 603774, https://doi.org/10.3389/fneur.2020.603774.

[35] F. Morani, S. Doccini, D. Galatolo, et al., Integrative organelle-based functional proteomics: in silico prediction of impaired functional annotations in SACS KO cell model, Biomolecules 12 (8) (2022), https://doi.org/10.3390/BIOM12081024.

[36] F. Morani, S. Doccini, R. Sirica, et al., Functional transcriptome analysis in ARSACS KO cell model reveals a role of sacsin in autophagy, Sci. Rep. 9 (1) (2019 Aug 15) 11878, https://doi.org/10.1038/s41598-019-48047-x.
[37] M. Moeton, R. Kanski, O.M. Stassen, J.A. Sluijs, D. Geerts, P. van Tijn, G. Wiche, M. E. van Strien, E.M. Hol, Silencing GFAP isoforms in astrocytoma cells disturbs laminin-dependent motility and cell adhesion, FASEB J. 28 (7) (2014 Jul) 2942–2954, https://doi.org/10.1096/fj.13-245837.
[38] J. Li, R. Wang, L. Yang, Q. Wu, Q. Wang, Z. Nie, Y. Yu, J. Ma, Q. Pan, Knockdown of nestin inhibits proliferation and migration of colorectal cancer cells, Int. J. Clin. Exp. Pathol. 8 (6) (2015 Jun 1) 6377–6386.
[39] C. De Pascalis, C. Pérez-González, S. Seetharaman, B. Boëda, B. Vianay, M. Burute, C. Leduc, N. Borghi, X. Trepat, S. Etienne-Manneville, Intermediate filaments control collective migration by restricting traction forces and sustaining cell-cell contacts, J. Cell Biol. 217 (9) (2018 Sep 3) 3031–3044, https://doi.org/10.1083/jcb.201801162.
[40] M.X. Cao, J. Boltze, S. Li, Factors regulating oligodendrocyte progenitor cell migration: from development to remyelination, Glia (2025 Jun 13), https://doi.org/10.1002/glia.70051.